

Aerosol light-scattering enhancement due to water uptake during TCAP campaign

G. Titos^{1,2}, A. Jefferson^{3,4}, P. J. Sheridan³, E. Andrews^{3,4}, H. Lyamani^{1,2}, L. Alados-Arboledas^{1,2}, and J. A. Ogren³

[1] {Instituto Interuniversitario de Investigación del Sistema Tierra en Andalucía, IISTA-CEAMA, Universidad de Granada, Junta de Andalucía, Granada, 18006, Spain}

[2] {Department of Applied Physics, University of Granada, Granada, 18071, Spain}

[3] {Earth System Research Laboratory, National Oceanic and Atmospheric Administration, Boulder, CO, 80305, United States}

[4] {Cooperative Institute for Research in Environmental Sciences, University of Colorado, Boulder, CO, 80305, United States}

Correspondence to: G. Titos (gtitos@ugr.es)

Abstract

Aerosol optical properties were measured by the DOE/ARM (US Department of Energy Atmospheric Radiation Measurements) Program Mobile Facility during the Two-Column Aerosol Project (TCAP) campaign deployed at Cape Cod, Massachusetts, for a one year period (from summer 2012 to summer 2013). Measured optical properties included aerosol light-absorption coefficient (σ_{ap}) at low relative humidity (RH) and aerosol light-scattering coefficient (σ_{sp}) at low and at RH values varying from 30 to 85%, approximately. Calculated variables included the single scattering albedo (SSA), the scattering Ångström exponent (SAE) and the scattering enhancement factor ($f(RH)$). Over the period of measurement, $f(RH=80\%)$ had a mean value of 1.9 ± 0.3 and 1.8 ± 0.4 in the PM_{10} and PM_1 fractions, respectively. Higher $f(RH=80\%)$ values were observed for wind directions from $0-180^\circ$ (marine sector) together with high SSA and low SAE values. The wind sector from 225 to 315° was identified as an anthropogenically-influenced sector, and it was characterized by smaller, darker and less hygroscopic aerosols. For the marine sector, $f(RH=80\%)$ was 2.2 compared with a value of 1.8

1 obtained for the anthropogenically-influenced sector. The air-mass backward trajectory
2 analysis agreed well with the wind sector analysis. It shows low cluster to cluster
3 variability except for air-masses coming from the Atlantic Ocean that showed higher
4 hygroscopicity. Knowledge of the effect of RH on aerosol optical properties is of great
5 importance for climate forcing calculations and for comparison of in-situ measurements
6 with satellite and remote sensing retrievals. In this sense, predictive capability of $f(\text{RH})$
7 for use in climate models would be enhanced if other aerosol parameters could be used
8 as proxies to estimate hygroscopic growth. Toward this goal, we propose an exponential
9 equation that successfully estimates aerosol hygroscopicity as a function of SSA at
10 Cape Cod. Further work is needed to determine if the equation obtained is valid in other
11 environments.

12

13 **1 Introduction**

14 The Earth's atmosphere plays an important role in the planetary energy budget through
15 different processes that shape the Earth's climate. Changes in its composition, even in
16 the less abundant components, like aerosols, can drive climate changes. Aerosol
17 particles actively scatter and absorb radiation as well as change the microphysical
18 properties of clouds. An important factor that can modify the role of aerosols in the
19 global energy budget is the relative humidity (RH). Aerosol particles can take up water,
20 become larger in size than their dry equivalents, and hence, scatter more light. Wet
21 particles may also have different refractive indices and angular scattering properties
22 than their dry counterparts. Continuous measurements of aerosol properties are typically
23 performed under dry conditions ($\text{RH} < 40\%$) as recommended by international networks
24 such as ACTRIS or GAW (WMO/GAW, 2003). These measurements at low RH can
25 differ from what would be observed at ambient conditions and thus difficult to relate to
26 observations of the radiative energy budget. Therefore, knowledge of the scattering
27 enhancement due to water uptake is of great importance in order to transform dry
28 measurements into more relevant ambient measurements, especially when comparing
29 in-situ with remote sensing measurements (e.g., Zieger et al., 2011; Zieger et al., 2012;
30 Estéve et al., 2012; Shinozuka et al., 2013) or for satellite retrievals (e.g., Wang and
31 Martin, 2007).

32 The effect of RH on the aerosol light-scattering coefficient can be determined by means
33 of a tandem nephelometer system (Covert et al., 1972; Fierz-Schmidhauser et al., 2010a,

1 and references therein). Typically, one nephelometer measures at a reference RH
2 (<40%) while the other nephelometer measures at a higher RH. The combination of
3 both measurements allows the determination of the scattering enhancement factor,
4 $f(\text{RH})$, defined as the ratio between the scattering coefficient at high RH and the
5 scattering coefficient at dry conditions. When these measurements are performed by
6 scanning the higher RH over a range of values instead of at constant RH, the evaluation
7 of $f(\text{RH})$ as a function of RH is possible. Different equations have been used to fit $f(\text{RH})$
8 versus RH. The most widely used equation is a two-parameter, power law fit (e.g.,
9 Hänel and Zankl, 1979; Clarke et al., 2002). This equation uses a fit parameter γ to
10 describe the humidity dependence of $f(\text{RH})$ for the entire RH range. The use of γ allows
11 the comparison of measurements taken at different RH values. Carrico et al. (2003)
12 describes several other fitting techniques as well, applied to different RH ranges.

13 Many studies have been published assessing the impact of RH on the aerosol light
14 scattering coefficient for different aerosol types such as urban (Yan et al., 2009), free
15 troposphere (Fierz-Schmidhauser et al., 2010b), continental (e.g., Sheridan et al., 2001;
16 Pan et al., 2009) and marine aerosols (e.g., McInnes et al., 1998; Fierz-Schmidhauser et
17 al., 2010c). Much of the recent research was performed in Central European sites
18 (Zieger et al., 2013) and was focused on short measurement campaigns of one to four
19 months duration. While there are a fair number of $f(\text{RH})$ ground based studies on a
20 variety of aerosol types, very few of them have provided information on the aerosol
21 scattering enhancement of fine mode aerosols; although some exceptions can be found
22 in the literature (e. g., McInnes et al., 1998; Koloutsou-Vakakis et al., 2001; Sheridan et
23 al., 2001; Carrico et al., 2003; Fierz-Schmidhauser et al., 2010a).

24 In this work, aerosol optical properties in two size ranges ($D_p < 1 \mu\text{m}$ and $D_p < 10 \mu\text{m}$)
25 were measured over a one year period at Cape Cod (Massachusetts, USA) during the
26 Two-Column Aerosol Project (TCAP) campaign. Information concerning aerosol
27 hygroscopicity is available for 7 months of the campaign. The main goals of this work
28 are to characterize the hygroscopic scattering enhancement during the TCAP campaign
29 and to explore the different situations and factors that led to changes in the
30 hygroscopicity, as well as to explore the use of dry optical properties as proxies to
31 estimate the hygroscopic enhancement.

32

33 **2 Experimental site and instrumentation**

2.1 Site description

The measurements presented in this study were conducted by the DOE/ARM (US Department of Energy Atmospheric Radiation Measurements) Program Mobile Facility (Miller and Slingo, 2007; Mather and Voyles, 2013) during the Two-Column Aerosol Project (TCAP) campaign (Kassianov et al., 2013) deployed at Cape Cod, Massachusetts. Cape Cod is a peninsula jutting out into the Atlantic Ocean in the easternmost portion of the state of Massachusetts, in the northeastern United States. The deployment was located in the northeastern part of the cape ($41^{\circ}59'36''$ N, $70^{\circ}03'01''$ W, 20 m a.s.l.), inside the Cape Cod National Seashore, and relatively close to large urban agglomerations such as Providence and Boston. Thus, due to its location, the site is subject to both clean and polluted conditions. The campaign started in the summer of 2012 and lasted until the summer of 2013; however, due to problems with the humidifier system, measurements of the hygroscopic enhancement are only available for approximately half of the campaign (from late September to late October 2012 and then from January to mid June 2013).

2.2 Instrumentation

Air sampling for all the instrumentation used in this study was obtained from the top of a 10 m high sampling stack of 20.3 cm in diameter. Airflow through this main stack is about 800 lpm. From this flow, 150 lpm flow through a 5.1 cm diameter stainless steel pipe in the center of this larger flow that then is divided into five 30-lpm sample lines. One of these sample lines goes to the Aerosol Observing System (AOS) instruments and the other 4 spare sample lines go out through a blower. A more detailed description of the sampling system can be found in Jefferson (2011).

The experimental set-up consists of two integrating nephelometers (TSI, model 3563) operated in series and separated by a humidifier system. Since no active drying of the aerosol sample is performed after humidification only the lower branch of the hysteresis curve can be captured with this set-up. The integrating nephelometer (TSI, model 3563) measures aerosol light-scattering (σ_{sp}) and hemispheric backscattering (σ_{bsp}) coefficients at three wavelengths (450, 550 and 700 nm). Instrument zero checks on filtered air were automatically performed hourly. Routine maintenance and instrument calibrations with CO_2 were performed 3 times; once in July, another in January and again in June. The nephelometers are downstream of a switched impactor system which toggles the aerosol size cut between $1.0 \mu m$ (PM_{1}) and $10 \mu m$ (PM_{10}) aerodynamic particle diameters every

1 30 minutes. The first nephelometer measures the aerosol light-scattering coefficient at
2 dry conditions ($RH < 40\%$) while the second nephelometer measures the aerosol light-
3 scattering coefficient at a controlled RH. The sampled aerosol was gently heated when
4 necessary to achieve a low relative humidity (RH) of 40% or below. The mean \pm
5 standard deviation of the temperature and relative humidity within the dry nephelometer
6 for the whole measurement campaign were $T = 26 \pm 4$ °C and $RH = 30 \pm 13$ %. In order to
7 minimize losses of volatile compounds the temperature of the sampled air was kept
8 below 35 °C (Bergin et al., 1997; ten Brink et al., 2000). Only 0.5% of the 1-min
9 observations occurred at temperatures above this value and these data were not further
10 considered in the study. The humidifier consists of two concentric tubes: the inner one
11 is a high-density porous polytetrafluoroethylene (PTFE) tube and the outer tube is a
12 stainless steel tube wrapped in a tape heater and insulation. A closed loop of water
13 circulates between the PTFE and the outer tube. As the water temperature increases,
14 water vapor moves through the semi-permeable PTFE membrane causing the RH of the
15 sample air to increase. The temperature of the water is regulated via a feedback system
16 between the downstream RH sensor, the PID (proportional-integral-derivative)
17 controller and the heater. Temperature and relative humidity sensors (Vaisala model
18 HMP110, accuracy of $\pm 3\%$ RH) are placed throughout the system: one of the sensors is
19 placed upstream of the impactor box and the other two sensors are placed immediately
20 downstream of the reference and humidified nephelometers. The internal nephelometer
21 TSI RH sensors are not used because of their slower time response and uncertainty. For
22 this reason, the RH inside the nephelometer was calculated from the dew point
23 temperature of the Vaisala sensor at the outlet of the humidified nephelometer and the
24 internal nephelometer temperature. The instruments reported results at 1-Hz resolution,
25 and the data were then averaged and recorded at 1 min resolution. The nephelometers
26 operated at a volumetric flow rate of 30 lpm. Non-idealities due to truncation errors and
27 the non-Lambertian light source were corrected according to Anderson and Ogren
28 (1998). The uncertainty in the aerosol light-scattering coefficient is about 7%
29 (Heintzenberg et al., 2006). Every hour the RH measurement cycle started with a zero
30 measurement and then in the humidified nephelometer the RH was increased stepwise
31 to 80-85% within 30 min, and then decreased back to RH values of about 40% or below
32 during the second half of the hour. The upward RH scan corresponded to the PM_{10} size
33 cut and the downward RH scan to PM_1 . When both nephelometers measured at dry
34 conditions ($RH < 40\%$) the two of them agreed well (PM_{10} : slope = 1.073 ± 0.001 ,

1 intercept = $0.48 \pm 0.02 \text{ Mm}^{-1}$ and $R^2 = 0.99$; PM_{10} : slope = 0.971 ± 0.004 , intercept =
2 $0.68 \pm 0.04 \text{ Mm}^{-1}$ and $R^2 = 0.77$ (for the 550 nm wavelength)).

3 The aerosol light absorption coefficient was measured with a Particle Soot Absorption
4 Photometer (PSAP). The method is based on the integrating plate technique in which
5 the change in optical transmission of a filter caused by particle deposition on the filter is
6 related to the light absorption coefficient of the deposited particles using Beer-Lambert
7 Law. Here, a 3-wavelength version of the PSAP has been used, with nominal
8 wavelengths of 467 nm, 531 nm, and 650 nm. The PSAP data were corrected according
9 to Bond et al. (1999) and Ogren (2010). The uncertainty of the PSAP absorption
10 measurement, after application of the transmission and scattering correction, is 20–30%
11 (Bond et al., 1999). The PSAP is also downstream of the switched impactors.

12 Ambient temperature, relative humidity, wind speed and direction were continuously
13 monitored using the surface meteorological instrumentation (MET) data from the ARM
14 AMF1 facility.

15 Air mass back trajectories were computed using the HYSPLIT4 model (Draxler et al.,
16 2009) version 4.9 and were used to support the interpretation of the data.

17

18 **3 Methodology**

19 Aerosol intensive properties, such as the single scattering albedo (SSA), the
20 hemispheric backscatter fraction (b), the submicron scattering fraction (R_{sp}) and
21 scattering Ångström exponent (SAE), were calculated from the aerosol scattering and/or
22 absorption coefficients.

23 The scattering Ångström exponent characterizes the wavelength dependence of σ_{sp} and
24 was calculated using the 700 nm and 450 nm wavelength pair using the following
25 equation:

$$26 \quad SAE(\lambda_1 - \lambda_2) = -(\log \sigma_{sp}(\lambda_1) - \log \sigma_{sp}(\lambda_2)) / (\log \lambda_1 - \log \lambda_2) \quad (1)$$

27 This variable increases with decreasing particle size and typically has values around 2
28 or higher when the scattering process is dominated by fine particles, while it is close to
29 0 when the scattering process is dominated by coarse particles (Delene and Ogren,
30 2002).

1 The submicron scattering fraction allows apportionment of light scattering into sub- and
2 super-micrometer aerosol mode. It was calculated for the 550 nm wavelength as
3 follows:

$$4 \quad R_{sp}(\lambda) = \sigma_{sp(Dp < 1 \mu m)}(\lambda) / \sigma_{sp(Dp < 10 \mu m)}(\lambda) \quad (2)$$

5 The hemispheric backscatter fraction is the fraction of radiation that is scattered back at
6 angles between 90-170°. This parameter increases with decreasing particle size.

$$7 \quad b(\lambda) = \sigma_{bsp}(\lambda) / \sigma_{sp}(\lambda) \quad (3)$$

8 The aerosol single scattering albedo at 550 nm wavelength is the ratio of the scattering
9 and extinction coefficients. It was calculated using the following formula:

$$10 \quad SSA(\lambda) = \sigma_{sp}(\lambda) / (\sigma_{sp}(\lambda) + \sigma_{ap}(\lambda)) \quad (4)$$

11 In order to determine SSA at 550 nm, the absorption coefficient measured with the
12 PSAP was interpolated to the 550 nm wavelength using the above described Ångström
13 formula. In this work, SSA(550), b(550), $R_{sp}(550)$ and SAE(450-700) refer always to
14 dry conditions and to the PM₁₀ size fraction.

15 To quantify the effect of water uptake in the aerosol light scattering coefficient, the
16 scattering enhancement factor f(RH) defined as the ratio of $\sigma_{sp}(\lambda)$ at a high and at
17 reference RH ($\lambda = 550$ nm in the present work) was used and calculated as follows:

$$18 \quad f(RH, \lambda) = \sigma_{sp}(RH, \lambda) / \sigma_{sp}(dry, \lambda) \quad (5)$$

19 This study uses the following two-parameter equation (Clarke et al., 2002; Carrico et
20 al., 2003) to describe the increase in aerosol scattering due to hygroscopic growth:

$$21 \quad f(RH) = a (1-RH)^{-\gamma} \quad (6)$$

22 where a is the intercept at RH = 0% and γ parameterizes the magnitude of the scattering
23 enhancement. To reduce the influence of instrument noise on the calculation, only
24 values of the dry scattering coefficient above 5 Mm⁻¹ were considered in the calculation
25 of f(RH). The constraints imposed for the fitting were a lower RH of 40%, a minimum
26 span of 30% RH in each scan, a minimum of 50% data coverage in each scan, the RH in
27 the reference nephelometer had to be below 40% and a fit R² value above 0.5. These
28 criteria were applied for PM₁₀ and PM₁ size fractions, with each size fraction fitted
29 separately. A total of 2952 (PM₁₀) and 1753 (PM₁) humidograms were successfully

1 fitted for each size respectively. Additionally, for each scan, $f(\text{RH})$ values were
2 calculated at $\text{RH}=80\%$ using equation 6, enabling comparison of scan hygroscopicity.

3 4 **4 Results and discussion**

5 **4.1 Overview of the campaign**

6 Mean ambient temperature and relative humidity during the campaign were 7 ± 6 °C and
7 80 ± 20 %. Both variables presented clear diurnal patterns with higher temperature and
8 lower RH values at midday. The wind speed ranged from calm winds up to values close
9 to 20 m/s during specific periods, showing a mean campaign value of 5 ± 3 m/s. Winds
10 from the west direction occurred more frequently. Figure 1 shows an overview of the
11 daily average aerosol light-scattering and absorption coefficients, $\sigma_{\text{sp}}(550)$ and $\sigma_{\text{ap}}(531)$,
12 single scattering albedo, $\text{SSA}(550)$, and scattering Ångström exponent, $\text{SAE}(450-700)$,
13 in the PM_{10} fraction. For the entire campaign, the $\sigma_{\text{sp}}(550)$ had a mean \pm standard
14 deviation value of 22 ± 15 Mm^{-1} and the corresponding values for $\sigma_{\text{ap}}(531)$ were 1.1 ± 0.9
15 Mm^{-1} . In general, the aerosol light absorption coefficient was very low during the
16 measurement period, especially compared with the scattering coefficient; the $\text{SSA}(550)$
17 had a mean value of 0.94 ± 0.04 . On the other hand, daily-average $\text{SSA}(550)$ values
18 ranged from 0.77 to 1.0, denoting periods where the contribution of absorption
19 increased. The campaign-averaged $\text{SAE}(450-700)$ was 1.8 ± 0.6 , which is quite high for a
20 coastal environment compared with literature values (e.g., Carrico et al., 1998; Fierz-
21 Schmidhauser et al., 2010b), and is an evidence of the influence of anthropogenic
22 aerosols at Cape Cod during TCAP campaign. In fact, the $\text{SAE}(450-700)$ showed a high
23 variability with daily values ranging from 0.6 to 3. The submicron scattering fraction
24 reported similar information with values ranging from 0.02 to 1 indicating different
25 atmospheric conditions dominated by different aerosol types (fine, coarse and mixed
26 particles). Concerning the backscatter fraction, this variable had a mean campaign value
27 of 0.13 ± 0.02 . The $\text{SAE}(450-700)$, $R_{\text{sp}}(550)$ and $b(550)$ report similar information since
28 all three parameters are related to aerosol mean size (Fan et al., 2014). In fact, the
29 $\text{SAE}(450-700)$ had a strong correlation with R_{sp} ($R^2 = 0.81$) and a moderate correlation
30 with b ($R^2 = 0.5$), both at 550 nm. For this reason, in the following sections we will
31 focus on the scattering Ångström exponent as indicator of particle size.

1 None of the variables mentioned above showed a clear diurnal pattern, presenting very
2 small changes throughout the day. In addition, no clear temporal trend was observed
3 throughout the study period, although certain events of elevated $\sigma_{sp}(550)$ were observed
4 connected with high SSA(550) values and low SAE(450-700) values. These events
5 occurred under high wind speeds and were probably caused by sea salt particles (large
6 particles with minimal absorption). As an example, on 9 March the $\sigma_{sp}(550)$ reached its
7 maximum value (daily average of 84 Mm^{-1}). On this day the SSA had a mean value of 1
8 and the SAE was 0.75, suggesting that the aerosol optical properties were dominated by
9 coarse, purely scattering particles.

10 Figure 2 shows the aerosol light scattering enhancement factor $f(\text{RH}=80\%)$ (upper
11 panel) and the γ parameter (lower panel) calculated for the PM_{10} and PM_1 fractions at
12 550 nm (hereafter the wavelength will be omitted in the notation for simplicity). Over
13 the period of measurement, $f(\text{RH}=80\%)$ had a mean value of 1.9 ± 0.3 , with daily-mean
14 values ranging from 1.4 to 2.6 in the PM_{10} fraction. In the PM_1 fraction, $f(\text{RH}=80\%)$
15 had a mean value of 1.8 ± 0.4 and ranged from 1.2 to 3.4. Average γ values were 0.5 for
16 both size fractions but were relatively more variable in the PM_1 fraction (in PM_1 , daily γ
17 values ranged from 0.1 to 1.1, and in PM_{10} ranged from 0.2 and 0.9). The temporal
18 trend of $f(\text{RH}=80\%)$ and γ was similar in both size fractions, however, larger
19 differences between PM_{10} and PM_1 were observed for specific events. Specifically, on 9
20 March this difference was considerably larger with a mean daily $f(\text{RH}=80\%)$ of 3.1 in
21 PM_1 compared to 2.4 in PM_{10} . On this day, the air mass back-trajectories arriving at 500
22 m a.g.l. at the measurement station were coming from the Atlantic Ocean and traveled
23 at low altitude for the last three days, likely picking up sea salt particles. In order to
24 investigate in more detail the differences in the magnitude of the scattering
25 enhancement between the fine and coarse fractions, Figure 3 shows the hourly
26 $f(\text{RH}=80\%)$ values in PM_1 versus $f(\text{RH}=80\%)$ values in PM_{10} . Data when the SAE (at
27 dry conditions and in the PM_{10} fraction) was below and above 1, denoting a
28 predominance of larger and smaller particles, respectively, were fitted separately. The
29 graph shows that for situation dominated by aerosol sea salt ($\text{SAE} < 1$) the scattering in
30 the PM_1 fraction experienced a higher enhancement than in the PM_{10} fraction. This
31 same behavior was also found for the γ parameter (not shown). This indicates that small
32 sea salt particles have a larger scattering enhancement compared to coarse sea salt
33 particles. This result is supported by theoretical calculations of hygroscopic growth as a

1 function of particles size for common aerosol salts and acids made by Zieger et al.
2 (2013). These authors showed that $f(\text{RH}=85\%)$ increases with decreasing particle size
3 for all components studied, but increases more dramatically for NaCl, the largest
4 component in sea salt. On the other hand, this behavior can be also explained by a shift
5 in the size distribution to a scattering regime with a higher scattering efficiency when
6 the SAE is greater than 1.

7 A total of 2952 and 1753 RH scans in PM_{10} and PM_1 fractions, respectively, were fitted
8 according to the criteria explained in Section 3. Additional fits were performed for the
9 RH ranges below and above 65%. The values of $\gamma_{>65\%}$ and $\gamma_{<65\%}$ were used to identify
10 possible deliquescence transitions. Similar values of $\gamma_{>65\%}$ and $\gamma_{<65\%}$ indicate a
11 monotonic growth for the entire RH range, while distinct values ($\gamma_{<65\%} \ll \gamma_{>65\%}$)
12 indicate no significant enhancement below 65% and a large increase at an RH value
13 above 65%. For those cases in which $\gamma_{<65\%} \ll \gamma_{>65\%}$ the fit using the entire RH range
14 underestimated $f(\text{RH})$ values at both low and high RH and overestimated $f(\text{RH})$ at the
15 transition RH (around 65-75% RH). To illustrate this, Figure 4a and Figure 4b show the
16 daily average humidograms for two different cases dominated by deliquescent and non-
17 deliquescent particles, respectively. Figure 4a shows 9 March daily average
18 humidogram scan ($\gamma = 0.8$, $\gamma_{<65\%} = 0.4$ and $\gamma_{>65\%} = 1.1$) and Figure 4b shows the daily
19 average humidogram scan of 31 May ($\gamma = 0.3$, $\gamma_{<65\%} = 0.3$ and $\gamma_{>65\%} = 0.4$). On 9 March
20 the scattering enhancement for $\text{RH}>65\%$ was almost three fold the enhancement for
21 $\text{RH}<65\%$. As mentioned before, during this day there was a predominance of non-
22 absorbing coarse particles (mean $\text{SAE}(450-700) = 0.75$ and $\text{SSA}(550) = 1$), suggesting a
23 clear contribution of deliquescent sea salt particles. On the other hand, on 31 May the
24 scattering enhancement was similar for both RH ranges. Slightly darker, non-
25 deliquescent fine mode particles dominated the aerosol on 31 May ($\text{SAE}(450-700) =$
26 1.8 , $\text{SSA}(550) = 0.91$) compared with the previous case. Concerning the “a” parameter,
27 it varies with the aerosol transmission efficiency through the humidifier and goodness
28 of the power law fit. Differences between the experimental and ideal value of “a” are
29 expected since the “a” value will depend also on aerosol losses in the dry nephelometer
30 and in the humidifier system. In this study, fitting the whole RH range for deliquescent
31 aerosols seems to be inadequate. Nevertheless, fitting $f(\text{RH})$ to multiple RH ranges
32 offers information on aerosol deliquescence properties.

4.2 Influence of wind speed and direction on the aerosol hygroscopicity

In order to evaluate the influence of wind speed and direction on aerosol hygroscopic properties, Figure 5 shows bivariate plots of $f(\text{RH}=80\%)$, γ , SSA(550) and SAE(450-700) as a function of wind speed and direction (Openair software, Carslaw and Ropkins, 2012). Both $f(\text{RH}=80\%)$ and γ increased with wind speed. SSA(550) and SAE(450-700) have opposite trends to each other, with increasing SSA(550) values and decreasing SAE(450-700) with wind speed. These plots show that there is a region between approximately 225 and 315°, characterized by lower SSA(550) and higher SAE(450-700), probably influenced by anthropogenic air from the populated urban areas of Providence and Boston. In contrast, the region from 0 to 180°, characterized by higher SSA(550) and lower SAE(450-700), can be considered as marine dominated aerosols from the North Atlantic ocean. According to these results, two wind sectors have been considered for further investigation: the marine sector (0-180°) and the anthropogenically-influenced sector (225-315°). For this analysis, only wind speed values above 5 m/s were considered in order to avoid local influences. The marine wind sector was characterized by slightly higher temperatures and RH values (median values: $T = 4.9$ and $\text{RH} = 89\%$) than the anthropogenically-influenced wind sector ($T = 2.4$ °C and $\text{RH} = 58\%$). This last sector also showed a higher variability in the temperature values. Table 1 summarizes the mean and standard deviation of the aerosol optical parameters for each sector. There is a clear difference between both wind sectors when looking at the aerosol intensive properties. The anthropogenically-influenced sector was characterized by smaller and more absorbing particles with similar $f(\text{RH}=80\%)$ for both size fractions. Furthermore, for the anthropogenically-influenced sector, $\gamma_{>65\%}$ and $\gamma_{<65\%}$ were very similar denoting no distinct deliquescent behavior. The marine sector presented very different properties compared with the anthropogenic sector: it was characterized by larger and very weakly absorbing particles (see Table 1). The $f(\text{RH}=80\%)$ was higher in the PM_1 than PM_{10} fraction, denoting a larger scattering enhancement in the fine mode. In addition, $\gamma_{>65\%}$ was considerably higher (0.9 ± 0.2) than $\gamma_{<65\%}$ (0.4 ± 0.1), evidence of deliquescent aerosols. Carrico et al. (2000) also observed a higher scattering enhancement for clean marine conditions than for polluted situations (see Table 2) in Sagres (Portugal) which agrees with the results obtained in this section (Table 1) and those shown in Figure 3. The $f(\text{RH})$ values reported here for clean and

1 anthropogenically influenced marine aerosols are in agreement with the range of values
2 reported in the literature (Table 2).

3 **4.3 Air-mass trajectories classification**

4 A cluster analysis of 3-day air mass backtrajectories arriving at Cape Cod at 500 m
5 a.g.l. at 00, 06, 12 and 18 GMT using HYSPLIT4 model (Draxler et al., 2009) version
6 4.9 was performed to identify the main air masses types affecting the area and their
7 respective aerosol optical properties. This method is based on the geometric distance
8 between individual trajectories and it takes into account speed and direction of the
9 trajectory and height at the arriving location. A total of 1344 backward trajectories were
10 used in the analysis. The number of clusters was selected according to the percent
11 change in total spatial variance (TSV). Large changes in the TSV were interpreted as
12 the merging of significantly different trajectories into the same cluster. According to
13 this criterion, the cluster analysis resulted in five clusters of backtrajectories for air
14 masses arriving at Cape Cod at low level. Figure 6 shows the clusters obtained with this
15 analysis and the average humidogram for each cluster. The humidograms represent
16 $f(\text{RH})$ averages in 2% RH size bins and the error bars represent the standard deviation in
17 the PM_{10} fraction. Table 3 shows, for each cluster, the mean and standard deviation of
18 the optical parameters. Clusters 1-4 exhibited similar aerosol optical properties with
19 only small differences. Cluster 5 was characterized by small $\text{SAE}(450-700)$ and high
20 $\text{SSA}(550)$, as well as by high γ and $f(\text{RH}=80\%)$ values. The air masses included in this
21 cluster came from the north-east, some of them originating as far away as Greenland,
22 passing over sparsely-populated regions and the Atlantic Ocean. The high $\text{SAE}(450-$
23 $700)$ for cluster 4 together with a lower $\text{SSA}(550)$ denotes an anthropogenic influence.
24 Clusters 3 and 4 had similar characteristics in terms of the aerosol optical properties (see
25 Figure 6 and Table 3). Both clusters comprise continental air masses. Clusters 1 and 2
26 had hybrid properties: with a predominance of larger particles compared to cluster 3 and
27 4 and with higher SSA values. This is probably because the air masses in clusters 1 and
28 2 passed over open Ocean but originated in polluted continental regions. The cluster to
29 cluster variation in the aerosol optical properties can be explained by the degree of
30 anthropogenic and marine influence in the air masses included in each cluster.

31 **4.4 Relationship between γ and SSA and SAE**

32 Predictive capability and global coverage of aerosol hygroscopicity for use in climate
33 models would be enhanced if other aerosol parameters could be used as proxies to

1 estimate hygroscopic growth. Toward this goal, we examined covariances between γ
 2 and aerosol intensive properties. Figure 7 shows the frequency distribution of γ in the
 3 PM₁₀ fraction for different SAE and SSA ranges. Values of SAE(450-700) below 1
 4 denote a higher predominance of coarse particles and lower SSA(550) values indicate
 5 darker aerosols. From Figure 7b, it is clear that aerosols containing a higher fraction of
 6 absorbing particles (lower SSA) are less hygroscopic since the frequency distribution is
 7 shifted towards lower γ values. In contrast, Figure 7a suggest that when coarse aerosols
 8 predominate (SAE<1) the hygroscopic enhancement is larger. In general, γ decreased as
 9 the contribution of coarse particles decreased, that is, as SAE increased (the correlation
 10 coefficient of γ versus SAE was R = -0.77). This result contrasts with the result of
 11 Zieger et al. (2010) that showed a decrease of γ for an increase in the contribution of
 12 coarse particles (R = 0.34), probably connected with compensating effects of different
 13 varying aerosol properties during their study.

14 Because the γ frequency distribution segregates well between high and low values of
 15 SSA and SAE, these variables seem to be good candidates as proxies to estimate the
 16 scattering enhancement due to water uptake. Based on the previous results, the
 17 following question arises: Can the aerosol hygroscopicity be predicted based on dry
 18 optical properties? To answer this question, Figure 8 (upper panel) shows γ versus
 19 SSA(550) where the color code represents the range of SAE(450-700). Figure 8a refers
 20 to γ in PM₁ and Figure 8b refers to γ in PM₁₀. In both γ graphs, SAE(450-700) and
 21 SSA(550) corresponds to the PM₁₀ size fraction and to dry conditions. The PM₁ γ was
 22 referenced to PM₁₀ SSA and SAE as a means to make the fits applicable to surface
 23 measurements which may have only PM₁₀ data and still differentiate the total and fine
 24 mode aerosol for models. As SSA(550) values increase the contribution of coarse
 25 particles also increases and these particles become more hygroscopic (bluish colors in
 26 Figure 8). The increase of γ with SSA in 550 nm wavelength is well described by the
 27 following exponential functions for the PM₁ (equation 7) and PM₁₀ (equation 8) size
 28 fractions respectively:

$$29 \quad \gamma = (3 \pm 5) \cdot 10^{-15} e^{\frac{SSA}{(0.030 \pm 0.001)}} + (0.31 \pm 0.01) \quad (7)$$

$$30 \quad \gamma = (4 \pm 3) \cdot 10^{-9} e^{\frac{SSA}{(0.054 \pm 0.002)}} + (0.26 \pm 0.01) \quad (8)$$

31 The coefficient of determination was R² = 0.76 in PM₁ and R² = 0.77 in PM₁₀. The
 32 increase observed in γ for higher SSA(550) values is more pronounced in the PM₁ than

1 in the PM_{10} size fractions. Figure 8 (lower panel) shows the frequency distribution of
2 the residuals for the fit in PM_1 and in PM_{10} , respectively, in order to assess the quality
3 of the regression. About 79% of the γ values in PM_1 and 92% in PM_{10} were estimated
4 by the model with a difference of ± 0.15 in γ . The residuals did not exhibit any
5 dependence on SAE, suggesting that the exponential fit captures most of the covariance
6 between SAE and SSA. The potential of this model lies in its simplicity, as the aerosol
7 hygroscopicity can be estimated by a single parameter, the dry single scattering albedo.
8 Quinn et al. (2005) proposed a parameterization based on the aerosol chemical
9 composition, in particular, in the fraction of particulate organic matter to predict $f(RH)$.
10 Also based on the chemical composition, Garland et al. (2007) reported that the
11 $f(RH=80\%)$ varied linearly with the organic/inorganic content. However, measurements
12 of aerosol chemical composition are commonly performed once a week and integrated
13 over a 24 hour period whereas optical properties are continuously measured at high time
14 resolution. In this particular study, the coarse mode was predominantly dominated by
15 sea salt particles and the presence of other species that typically accumulate in the
16 coarse fraction like dust particles was negligible. Due to the similar characteristics of
17 sea salt and dust particles in terms of SAE and SSA, but the strong difference in the
18 hygroscopic behavior, the parameterization proposed in this study would fail under the
19 presence of both types of aerosols as pure dust aerosols does not experience significant
20 hygroscopic growth. The Cape Cod study may be considered as representative of an
21 aerosol from the Northern Atlantic coast with anthropogenic influence. The same
22 analysis needs to be applied to other regions and aerosol types to catalog exponential fit
23 parameters of γ versus SSA over a variety of aerosol types and atmospheric conditions.

24

25 **5 Conclusions**

26 The measured $f(RH)$ dependency with RH during TCAP campaign can be well
27 described with an empirical two-parameter fit equation for both size fractions (PM_1 and
28 PM_{10}). During the study period, $f(RH=80\%)$ and the fit parameter γ in PM_{10} had a mean
29 value of 1.9 and 0.5, respectively. Two distinct sectors were identified according to
30 wind speed and direction. For the marine sector (wind speed above 5 m/s and wind
31 direction between 0 and 180 degrees), the γ parameter had a mean value of 0.7 ± 0.1 for
32 $\gamma_{>65\%}$, which was considerably higher than for $\gamma_{<65\%}$. The sharp increase in $f(RH)$ at an
33 RH above 65% indicated the aerosol deliquescence. The anthropogenically-influenced

1 sector (wind speed above 5 m/s and wind direction between 225 and 315 degrees) was
2 characterized by a predominance of smaller and darker aerosols with lower
3 hygroscopicity. The enhanced fine mode hygroscopic growth was more pronounced for
4 sea salt aerosol than for mixed or anthropogenic aerosol. The air-mass trajectory
5 classification analysis agreed with the wind sector analysis. Small differences were
6 found between clusters, with the exception of cluster 5 that corresponds to clean marine
7 air masses.

8 A clear relationship between the intensive parameters SSA and SAE with γ was
9 observed. The γ parameter increased for increasing SSA and decreasing SAE values,
10 that is, larger and less absorbing particles tended to be more hygroscopic. An
11 exponential equation which fit γ to a single parameter (the single scattering albedo) was
12 found to have a relatively low residual error, suggestion that SSA was a good proxy of
13 the aerosol scattering hygroscopic growth. The Cape Cod study represents aerosol from
14 a Northern Atlantic coastal site with influence of marine and anthropogenic aerosols.
15 The same analysis needs to be applied to other regions and aerosol types to catalog
16 exponential fit parameters of γ versus SSA over a variety of aerosol types and
17 atmospheric conditions. This particular study had a strong covariance between SSA and
18 SAE, which allowed a reduction in the γ fit to a single parameter, SSA. Other sites with
19 smoke, dust or with strong differences in aerosol composition between the fine and
20 coarse mode may require more fit parameters.

21

22 **Acknowledgments**

23 This research was funded by the NOAA Climate Program using measurements funded
24 by the U.S. Department of Energy Atmospheric System Research program. The authors
25 would like to express their gratitude to the NOAA Air Resources Laboratory (ARL) for
26 the provision of the HYSPLIT transport and dispersion model. We would like to thank
27 also the Openair project. G. Titos was funded by Spanish Ministry of Economy and
28 Competitiveness – Secretariat of Science, Innovation and Development under grants
29 BES-2011-043721 and EEBB-I-13-06456, and projects P10-RNM-6299, CGL2010-
30 18782 and EU INFRA-2010-1.1.16-262254.

31

32

1

2 **References**

- 3 Anderson, T.L., and Ogren, J. A.: Determining aerosol radiative properties using the
4 TSI 3563 integrating nephelometer, *Aerosol Sci. Technol.*, 29, 57–69, 1998.
- 5 Bergin, M. H., Ogren, J. A., Schwartz, S.E. and McInnes, L. M.: Evaporation of
6 ammonium nitrate aerosol in a heated nephelometer: Implications for field
7 measurements. *Environ. Sci. Technol.*, 31, 2878–2883, 1997. Bond, T. C., Anderson, T.
8 L. and Campbell, D.: Calibration and intercomparison of filter-based measurements of
9 visible light absorption by aerosols. *Aerosol Sci. Technol.*, 30, 582– 600, 1999.
- 10 Carrico, C.M., Rood, M.J. and Ogren, J.A.: Aerosol light scattering properties at Cape
11 Grim, Tasmania, during the First Aerosol Characterization Experiment (ACE 1), *J.*
12 *Geophys. Res.*, 103, D13, 16565-16574, 1998.
- 13 Carrico, C. M., Rood, M. J., Ogren, J. A., Neusüb, C., Wiedensohler, A. and
14 Heintzenberg, J.: Aerosol optical properties at Sagres, Portugal during ACE-2, *Tellus*,
15 52B, 694-715, 2000.
- 16 Carrico, C. M., Kus, P., Rood, M. J., Quinn, P. K. and Bates, T. S.: Mixtures of
17 pollution, dust, sea salt, and volcanic aerosol during ACE-Asia: Radiative properties as
18 a function of relative humidity, *J. Geophys. Research.*, 108, D23, 8650, 2003.
- 19 Carslaw, D. C. and Ropkins, K.: Openair- An R package for air quality data analysis,
20 *Environmental Modelling & Software*, 27-28, 52-61, 2012.
- 21 Clarke, A. D., Howell, S., Quinn, P. K., Bates, T. S., Ogren J. A., Andrews, E.,
22 Jefferson, A., Massling, A., Mayol-Bracero, O., Maring, H., Savoie, D., and Cass, G.:
23 INDOEX aerosol: A comparison and summary of chemical, microphysical, and optical
24 properties observed from land, ship, and aircraft, *J. Geophys. Res.*, 107, 8033,
25 doi:803310.1029/2001JD000572, 2002.
- 26 Covert, D. S., Charlson, R. J. and Ahlquist, N. C.: A study of the relationship of
27 chemical composition and humidity to light scattering by aerosols, *Journal of Applied*
28 *Meteorology*, 11, 968-976, 1972.
- 29 Delene, D. J. and Ogren, J. A.: Variability of Aerosol Optical Properties at Four North
30 American Surface Monitoring Sites, *J. Atmos. Sci.*, 59, 1135–1149, 2002.

1 Draxler, R.R., Stunder, B., Rolph, G. and Taylor, A.: HYSPLIT4 User's Guide. NOAA
2 Air Resources Laboratory, 2009.

3 Estéve, A. R., Ogren, J. A., Sheridan, P. J., Andrews, E., Holben, B. N. and Utrillas, M.
4 P.: Sources of discrepancy between aerosol optical depth obtained from AERONET and
5 in-situ aircraft profiles, *Atmos. Chem. Phys.*, 12, 2987-3003, 2012.

6 Fan, X., Chen, H., Xia, X., Li, Z. and Cribb, M.: Aerosol optical properties from the
7 Atmospheric Radiation Measurement Mobile Facility at Shouxian, China, *J. Geophys.*
8 *Res.*, 115, D00K33, doi:10.1029/2010JD014650, 2010.

9 Fierz-Schmidhauser, R., Zieger, P., Wehrle, G., Jefferson, A., Ogren, J.A.,
10 Baltensperger, U. and Weingartner, E.: Measurement of relative humidity dependent
11 light scattering of aerosols, *Atmos. Meas. Tech.*, 3, 39-50, 2010a.

12 Fierz-Schmidhauser, R., Zieger, P., Gysel, M., Kammermann, L., DeCarlo, P. F.,
13 Baltensperger, U. and Weingartner, E.: Measured and predicted aerosol light scattering
14 enhancement factors at the high alpine site Jungfraujoch, *Atmos. Chem. Phys.*, 10,
15 2319-2333, 2010b.

16 Fierz-Schmidhauser, R., Zieger, P., Vaishya, A., Monahan, C., Bialek, J., O'Dowd, C.
17 D., Jennings, S. G., Baltensperger, U. and Weingartner, E.: Light scattering
18 enhancement factors in the marine boundary layer (Mace Head, Ireland), *J. Geophys.*
19 *Res.*, 115, D20204, 2010c.

20 Garland, R. M., Ravishankara, A. R., Lovejoy, E. R., Tolbert, M. A. and Baynard, T.:
21 Parameterization for the relative humidity dependence of light extinction: Organic-
22 ammonium sulfate aerosol, *J. Geophys. Res.*, 112, D19303, 2007.

23 Gassó, S., Hegg, D. A., Covert, D. S., Collins, D., Noone, K. J., Öström, E., Schmid, B.,
24 Russell, P. B., Livingston, J. M., Durkee, P. A. and Jonsson, H.: Influence of humidity
25 on the aerosol scattering coefficient and its effect on the upwelling radiance during
26 ACE-2, *Tellus*, 52B, 546-567, 2000.

27 Hänel, G. and Zankl, B.: Aerosol size and relative humidity: Water uptake by mixtures
28 of salts, *Tellus*, 31, 478-486, 1979.

29 Hegg, D. A., Covert, D. S., Rood, M. J. and Hobbs, P. V.: Measurements of aerosol
30 optical properties in marine air, *J. Geophys. Res.*, 101, D8, 12893-12903, 1996.

1 Heintzenberg, J., Wiedensohler, A., Tuch, T. M., Covert, D. S., Sheridan, P., Ogren, J.
2 A., Gras, J., Nessler, R., Kleefeld, C., Kalivitis, N., Aaltonen, V., Wilhelm, R. T., and
3 Havlicek, M.: Intercomparisons and aerosol calibrations of 12 commercial integrating
4 nephelometers of three manufacturers, *J. Atmos. Ocean. Tech.*, 23, 902–914, 2006.

5 Jefferson, A.: Aerosol Observing System (AOS) Handbook, U. S. Department of
6 Energy, DOE/SC- ARM/TR-014, (Available at
7 http://www.arm.gov/publications/tech_reports/handbooks/aos_handbook.pdf), 2011.

8 Kassianov, E., Barnard, J., Pekour, M., Berg, L. K., Fast, J., Michalsky, J., Lantz, K.
9 and Hodges, G.: Temporal variability of aerosol properties during TCAP: Impact on
10 radiative forcing, *Proc. SPIE8890*, doi:10.1117/12.2029355, 2013.

11 Koloutsou-Vakakis, S., Carrico, C. M., Kus, P., Rood, M. J., Li, Z., Shrestha, R., Ogren,
12 J. A., Chow, J. C. and Watson, G.: Aerosol properties at a midlatitude Northern
13 Hemisphere continental site, *J. Geophys. Res.*, 106, D3, 3019-3032, 2001.

14 Kotchenruther, R. A., Hobbs, P. V. and Hegg, D. A.: Humidification factors for
15 atmospheric aerosols off the mid-Atlantic coast of the United States, *J. Geophys. Res.*,
16 104, D2, 2239-2251, 1999.

17 Li-Jones, X., Maring, H. B. and Propero, J. M.: Effect of relative humidity on light
18 scattering by mineral dust aerosol as measured in the marine boundary layer over the
19 tropical Atlantic Ocean. *J. Geophys. Res.*, 103, D23, 31113-31121, 1998.

20 Mather, J. H. and Voyles, J. W.: The Arm Climate Research Facility: A Review of
21 Structure and Capabilities. *Bull. Amer. Meteor. Soc.*, 94, 377–392, doi:
22 <http://dx.doi.org/10.1175/BAMS-D-11-00218.1>, 2013.

23 Miller, M. A. and Slingo, A.: The ARM Mobile Facility and its first international
24 deployment: Measuring Radiative Flux Divergence in West Africa. *Bull. Amer. Meteor.*
25 *Soc.*, 88, 1299-1244, doi:10.1175/BAMS-88-8-1229, 2007.

26 McInnes, L., Bergin, M., Ogren, J. A. and Schwartz, S.: Apportionment of light
27 scattering and hygroscopic growth to aerosol composition, *Geophys. Res. Lett.*, 25, 4,
28 513-516, 1998.

29 Ogren, J. A.: Comment on “Calibration and Intercomparison of Filter-Based
30 Measurements of Visible Light Absorption by Aerosols”, *Aerosol Sci. Tech.*, 44:589-
31 591, 2010.

1 Pan, X. L., Yan, P., Tang, J., Ma, J. Z., Wang, Z. F., Gbaguidi, A. and Sun, Y. L.:
2 Observational study of influence of aerosol hygroscopic growth on scattering coefficient
3 over rural area near Beijing mega-city, *Atmos. Chem. Phys.*, 9, 7519-7530, 2009.

4 Quinn, P. K., Bates, T. S., Baynard, T., Clarke, A. D., Onasch, T. B., Wang, W., Rood,
5 M. J., Andrews, E., Allan, J., Carrico, C. M., Coffman, D. and Wornsnop, D.: Impact of
6 particulate organic matter on the relative humidity dependence of light scattering: A
7 simplified parameterization, *Geophys. Res. Lett.*, 32, L22809, 2005.

8 Sheridan, P.J., Delene, D. J. and Ogren, J. A.: Four years of continuous surface aerosol
9 measurements from the Department of Energy's Atmospheric Radiation Measurement
10 Program Southern Great Plains Cloud and Radiation Testbed site, *J. Geophys. Res.*,
11 106, D18, 20735-20747, 2001.

12 Sheridan, P. J., Jefferson, A. and Ogren, J. A.: Spatial variability of submicrometer
13 aerosol radiative properties over the Indian Ocean during INDOEX, *J. Geophys. Res.*,
14 107, D19, 8011, 2002.

15 Shinozuka, Y., Johnson, R. R., Flynn, C. J., Russell, P. B., Schmid, B., Redemann, J.,
16 Dunagan, S. E., Kluzek, C. D., Hubbe, J. M., Segal-Rosenheimer, M., Livingston, J. M.,
17 Eck, T. F., Wagener, R., Gregory, L., Chand, D., Berg, L. K., Rogers, R. R., Ferrare, R.
18 A., Hair, J. W., Hostetler, C. A. and Burton, S. P.: Hyperspectral aerosol optical depths
19 from TCAP flights, *J. Geophys. Res.*, Accepted, doi: 10.1002/2013JD020596, 2013.

20 ten Brink, H. M., Khlystov, A., Kos, G. P. A., Tuch, T., Roth, C. and Kreyling, W.: A
21 high flow humidograph for testing the water uptake by ambient aerosol. *Atmos.*
22 *Environ.*, 34, 4291-4300, 2000. Wang, J. and Martin, S. T.: Satellite characterization of
23 urban aerosols: Importance of including hygroscopicity and mixing state in the retrieval
24 algorithms, *J. Geophys. Res.*, 112, D17203, 2007.

25 WMO/GAW: Aerosol measurement procedures guidelines and recommendations,
26 GAWRep. 153, World Meteorol. Organ., Geneva, Switzerland. (Available at
27 <http://wdca.jrc.it/data/gaw153.pdf>), 2003.

28 Yan, P., Pan, X., Tang, J., Zhou, X., Zhang, R. and Zeng, L.: Hygroscopic growth of
29 aerosol scattering coefficient: A comparative analysis between urban and suburban sites
30 at winter in Beijing, *Particuology*, 7, 52-60, 2009.

1 Zieger, P., Fierz-Schmidhauser, R., Gysel, M., Ström, J., Henne, S., Yttri, K.,
2 Baltensperger, U., and Weingartner E.: Effects of relative humidity on aerosol light
3 scattering in the Arctic, *Atmos. Chem. Phys.*, 10(8), 3875–3890, doi:10.5194/acp-10-
4 3875-2010, 2010.

5 Zieger, P., Weingartner, E., Henzing, J., Moerman, M., de Leeuw, G., Mikkilä, J., Ehn,
6 M., Petäjä, T., Clémer, K., van Roozendaal, M., Yilmaz, S., Frieß, U., Irie, H., Wagner,
7 T., Shaiganfar, R., Beirle, S., Apituley, A., Wilson, K., and Baltensperger, U.:
8 Comparison of ambient aerosol extinction coefficients obtained from in-situ, MAX-
9 DOAS and LIDAR measurements at Cabauw, *Atmos. Chem. Phys.*, 11, 2603-2624,
10 2011.

11 Zieger, P., Kienast-Sjögren, E., Starace, M., von Bismarck, J., Bukowiecki, N.,
12 Baltensperger, U., Wienhold, F., Peter, T., Ruhtz, T., Collaud Coen, M., Vuilleumier,
13 L., Maier, O., Emili, E., Popp, C. and Weingartner E.: Spatial variation of aerosol
14 optical properties around the high-alpine site Jungfraujoch (3580 m a.s.l.), *Atmos.*
15 *Chem. Phys.*, 12, 7231–7249, doi: 10.5194/acp-12-7231-2012, 2012.

16 Zieger, P., Fierz-Schmidhauser, R., Weingartner, E. and Baltensperger, U.: Effects of
17 relative humidity on aerosol light scattering: results from different European sites,
18 *Atmos. Chem. Phys.*, 13, 10609-10631, 2013.

19

20

21

22

23

24

25

26

27

28

29

1 Table 1. Mean and standard deviation of single scattering albedo, scattering Ångström
 2 exponent, γ parameter, $\gamma_{>65\%}$, $\gamma_{<65\%}$ and scattering enhancement factor at 80% RH for
 3 PM₁₀ fraction and scattering enhancement factor at 80% RH for PM₁ fraction for the
 4 two wind sectors. All the variables refer to 550 nm except the scattering Ångström
 5 exponent that has been calculated between 450 and 700 nm.

Sector	SSA	SAE	γ	$\gamma_{>65\%}$	$\gamma_{<65\%}$	f(RH=80%)	f(RH=80%) in PM ₁
Anthro- pogenic	0.93±0.03	1.8±0.5	0.4±0.1	0.5±0.2	0.4±0.1	1.8±0.2	1.7±0.2
Marine	0.98±0.02	0.9±0.3	0.7±0.1	0.9±0.2	0.4±0.1	2.2±0.3	2.5±0.6

6
7
8
9
10
11
12
13
14
15
16
17
18
19
20
21
22
23

1 Table 2. Hygroscopic growth factors reported in the literature for marine environments.
 2 The values of $f(\text{RH})$ corresponds to the ratio of the aerosol light scattering coefficients
 3 (near 550 nm wavelength) at high RH (85% unless noted: *RH = 82%, **RH=80%) and
 4 at dry conditions (RH<40%). All samples were taken with size cut (D_p) of 10 μm unless
 5 specifically noted.

Source	Location	Year	$f(\text{RH})$	Notes
<i>Hegg et al. (1996a)</i>	eastern North Pacific	1994		No D_p cut
	Ocean		2.3**	Clean marine
<i>Li-Jones et al. (1998)</i>	Barbados, West Indies	1994	1.8**	Sea salt
<i>Carrico et al. (1998)</i>	Cape Grim, Tasmania	1995	1.98*	Clean marine
<i>McInnes et al. (1998)</i>	Sable Island, Canada	1996		$D_p < 1 \mu\text{m}$
			2.7	Marine
			1.7	Polluted
<i>Kotchenruther et al. (1999)</i>	western North Atlantic Ocean	1996		$D_p < 4 \mu\text{m}$,
			1.81**	"less anthropogenic"
<i>Carrico et al. (2000)</i>	Sagres, Portugal	1997		$D_p < 10 \mu\text{m}$
			1.69*	Clean
			1.46*	Polluted
				$D_p < 1 \mu\text{m}$
			1.86*	Clean
<i>Gassó et al. (2000)</i>	eastern North Atlantic Ocean	1997		$D_p < 2.5 \mu\text{m}$
			2.0**	Polluted
			2.5**	Clean
<i>Sheridan et al. (2002)</i>	Indian Ocean	1999		$D_p < 1 \mu\text{m}$

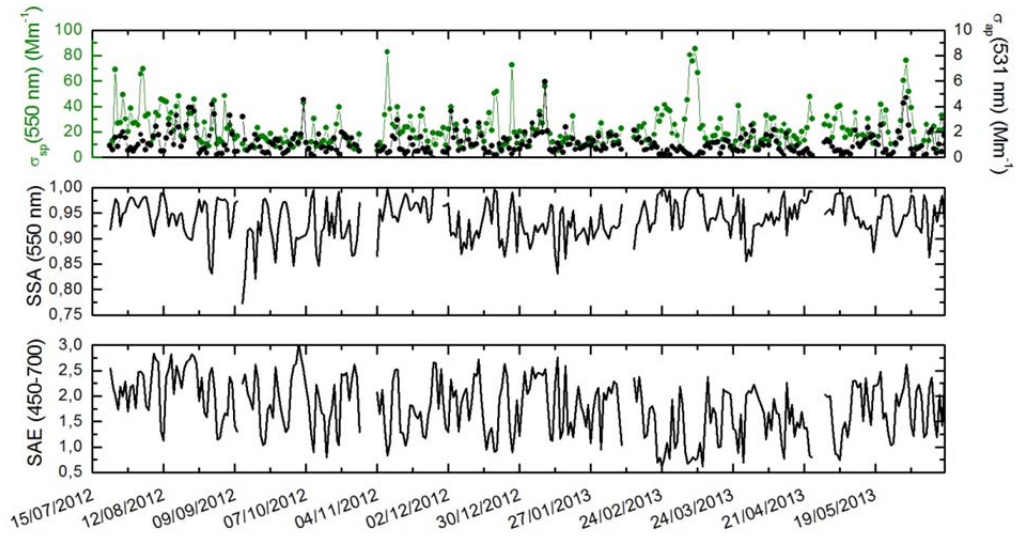
	Indian Ocean (North)		1.55	Polluted
	Indian Ocean (Central)		1.69 2.07	Polluted Clean marine
	Southern Hemisphere			
<i>Carrico et al. (2003)</i>	Asia/Pacific region	2001		$D_p < 10 \mu\text{m}$
			2.45*	Marine
			2.24*	Polluted
				$D_p < 1 \mu\text{m}$
			2.95*	Marine
			2.52*	Polluted
<i>Fierz-Schmidhauser et al. (2010b)</i>	Mace Head, Ireland	2009	2.2	Clean
			1.8	Polluted
<i>Zieger et al. (2011)</i>	Cabauw, The Netherlands	2009	3	Maritime
<i>This study</i>	Cape Cod, MA	2012- 2013		$D_p < 10 \mu\text{m}$
			2.2**	Clean marine
			1.8**	Anthropogenic
				$D_p < 1 \mu\text{m}$
			2.5**	Clean marine
			1.7**	Anthropogenic

1
2
3
4
5

1 Table 3. Mean and standard deviation of single scattering albedo, scattering Ångström
 2 exponent, γ parameter, $\gamma_{>65\%}$, $\gamma_{<65\%}$ and scattering enhancement factor at 80% RH for
 3 the five clusters. All the variables refer to PM₁₀ unless specifically noted and to 550 nm
 4 except the scattering Ångström exponent that has been calculated between 450 and 700
 5 nm.

Cluster	SSA	SAE	γ	$\gamma_{>65\%}$	$\gamma_{<65\%}$	f(RH=80%)	f(RH=80%) in PM ₁
1	0.94±0.04	1.9±0.7	0.5±0.2	0.6±0.3	0.4±0.1	1.9±0.3	1.8±0.4
2	0.95±0.04	1.8±0.6	0.5±0.1	0.5±0.2	0.4±0.1	1.9±0.3	1.8±0.3
3	0.92±0.04	1.9±0.5	0.4±0.1	0.6±0.2	0.4±0.1	1.7±0.2	1.6±0.3
4	0.92±0.03	2.1±0.5	0.4±0.1	0.5±0.2	0.4±0.1	1.8±0.2	1.7±0.2
5	0.97±0.03	1.1±0.5	0.7±0.2	0.9±0.2	0.4±0.1	2.1±0.3	2.5±0.6

6
 7
 8
 9
 10
 11
 12
 13
 14
 15
 16
 17
 18
 19
 20
 21



1

2 Figure 1. Temporal evolution of the daily dry scattering and absorption coefficients
 3 (upper panel), the single scattering albedo (middle panel) and the scattering Ångström
 4 exponent (lower panel). All the parameters correspond to the PM₁₀ fraction. The date is
 5 in the format dd/mm/yyyy.

6

7

8

9

10

11

12

13

14

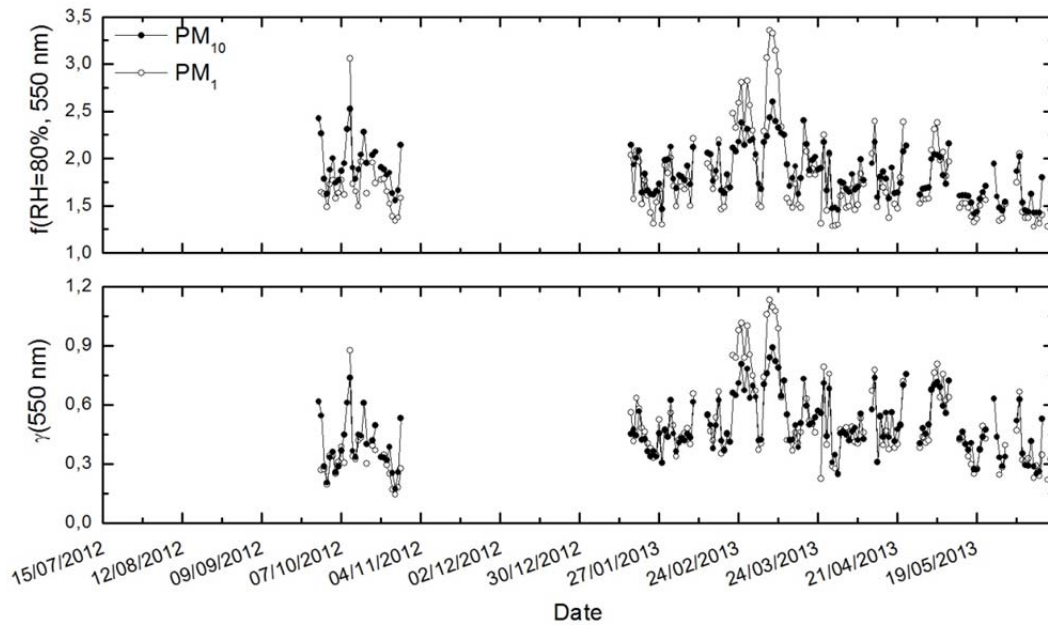
15

16

17

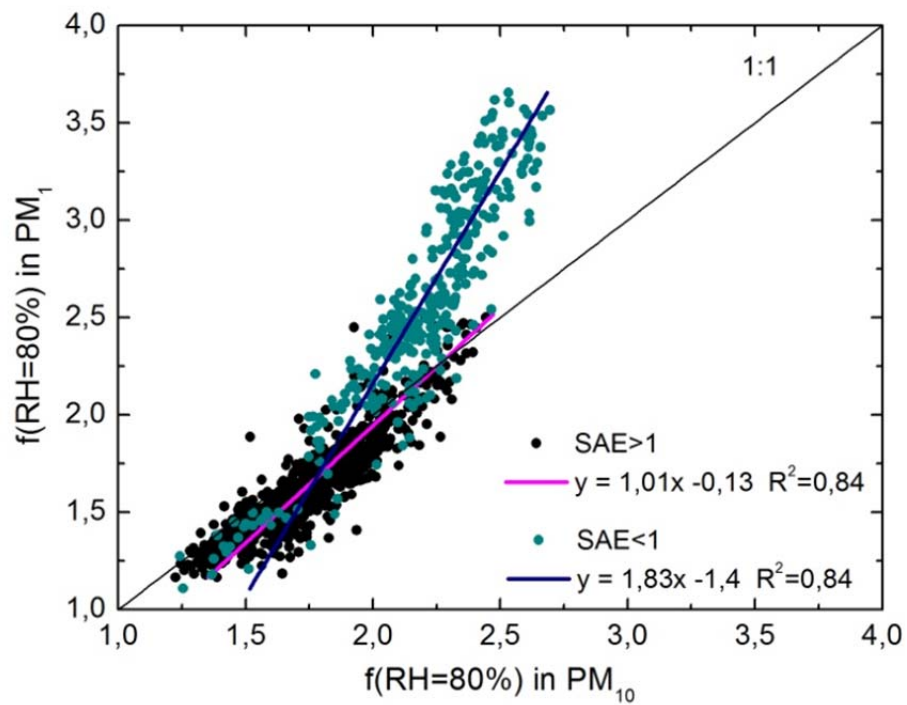
18

19



1
 2 Figure 2. Temporal evolution of the daily scattering enhancement factor at 80% relative
 3 humidity (upper panel) and the fit parameter γ (lower panel), for PM_{10} and PM_1
 4 fractions. The date is in the format dd/mm/yyyy.

5
 6
 7
 8
 9
 10
 11
 12
 13
 14
 15
 16
 17
 18



1

2 Figure 3. Scatter plot of the hourly average scattering enhancement factors at 80%
 3 relative humidity in the PM₁ fraction versus the same parameter in the PM₁₀ fraction.
 4 Data when the scattering Ångström exponent was below and above 1 were fitted
 5 separately.

6

7

8

9

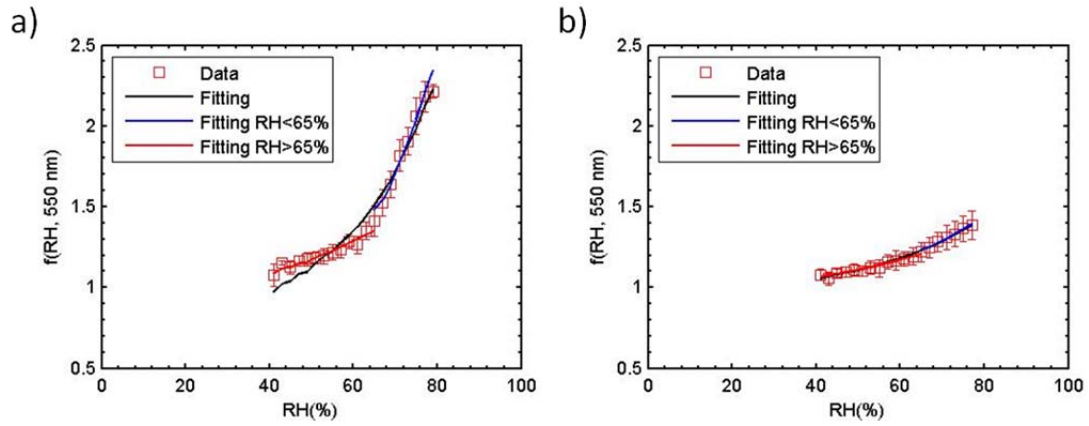
10

11

12

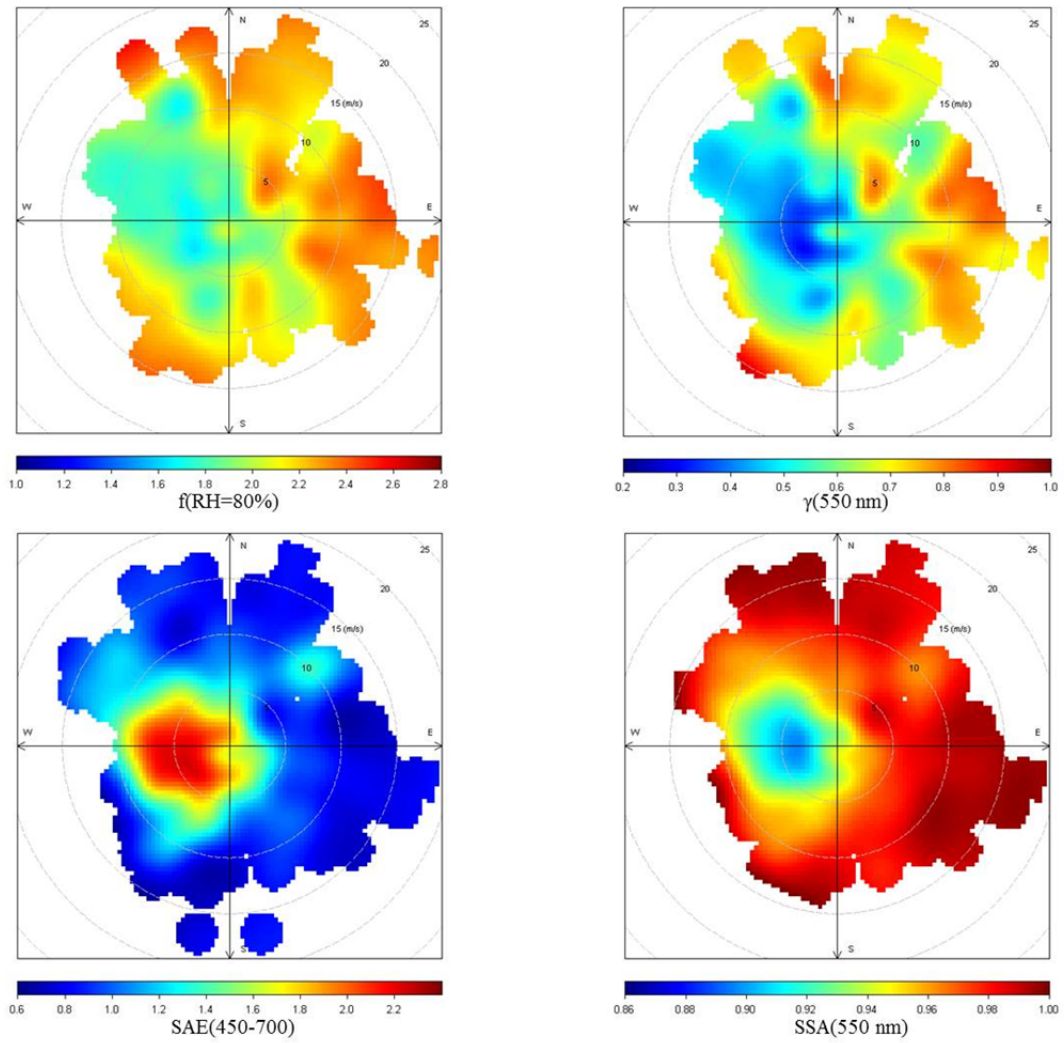
13

14



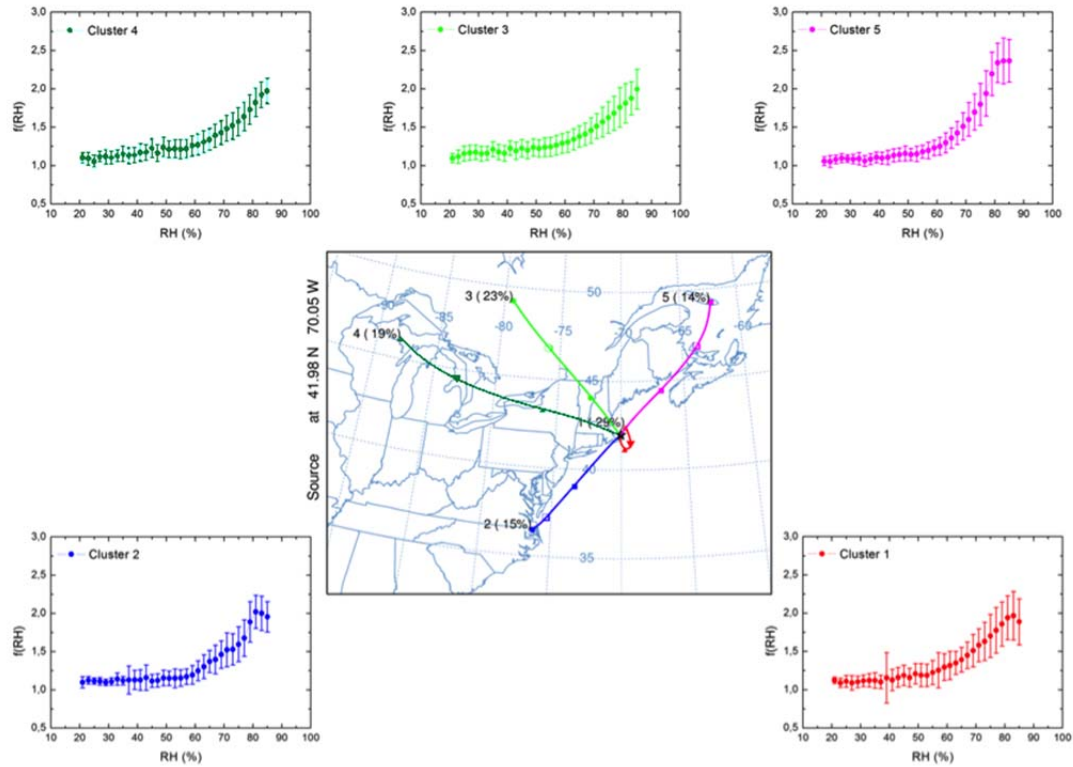
1
 2 Figure 4. Example humidograms of the scattering enhancement factor, given as daily
 3 averages where the error bars represent the standard deviation for the 9th of March (a)
 4 and the 31st of May (b). The black line denotes the γ fit for the entire RH range
 5 (RH>40%), the blue line denotes the γ fit for RH>65% and the red line the γ fit for the
 6 RH<65%.

7
 8
 9
 10
 11
 12
 13
 14
 15
 16
 17
 18
 19
 20
 21



1
2
3
4
5
6
7
8
9
10
11
12

Figure 5. Bivariate plots of the scattering enhancement factor at 80% RH, the γ parameter, single scattering albedo and scattering Ångström exponent as a function of wind speed and direction.



1

2 Figure 6. Clusterization of 3-days air masses backtrajectories arriving at Cape Cod at
 3 500 m a.g.l. at 00, 06, 12 and 18 GMT according to the HYSPLIT4 model (central
 4 panel) and average humidograms for each cluster. The error bars denote the standard
 5 deviation.

6

7

8

9

10

11

12

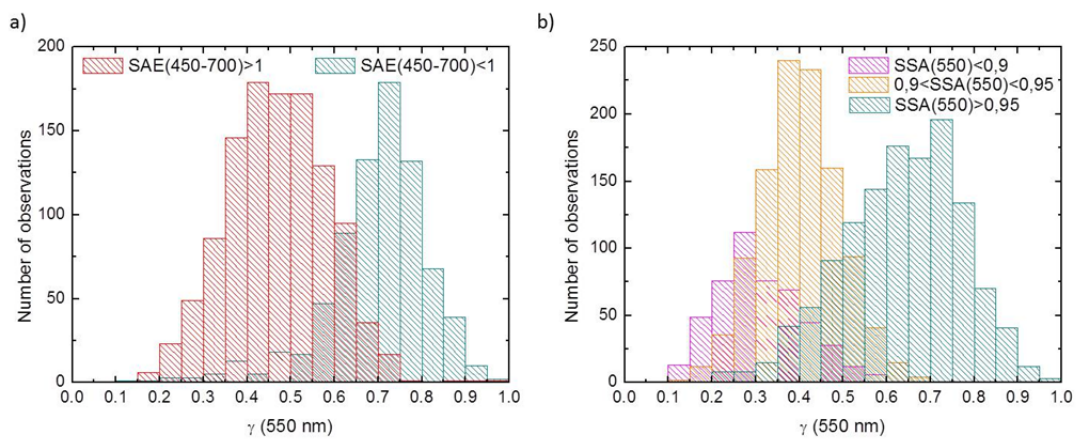
13

14

15

16

1



2

3 Figure 7. Frequency distribution of the γ parameter for different scattering Ångström
4 exponent (a) and single scattering albedo (b) ranges in the PM_{10} size fraction.

5

6

7

8

9

10

11

12

13

14

15

16

17

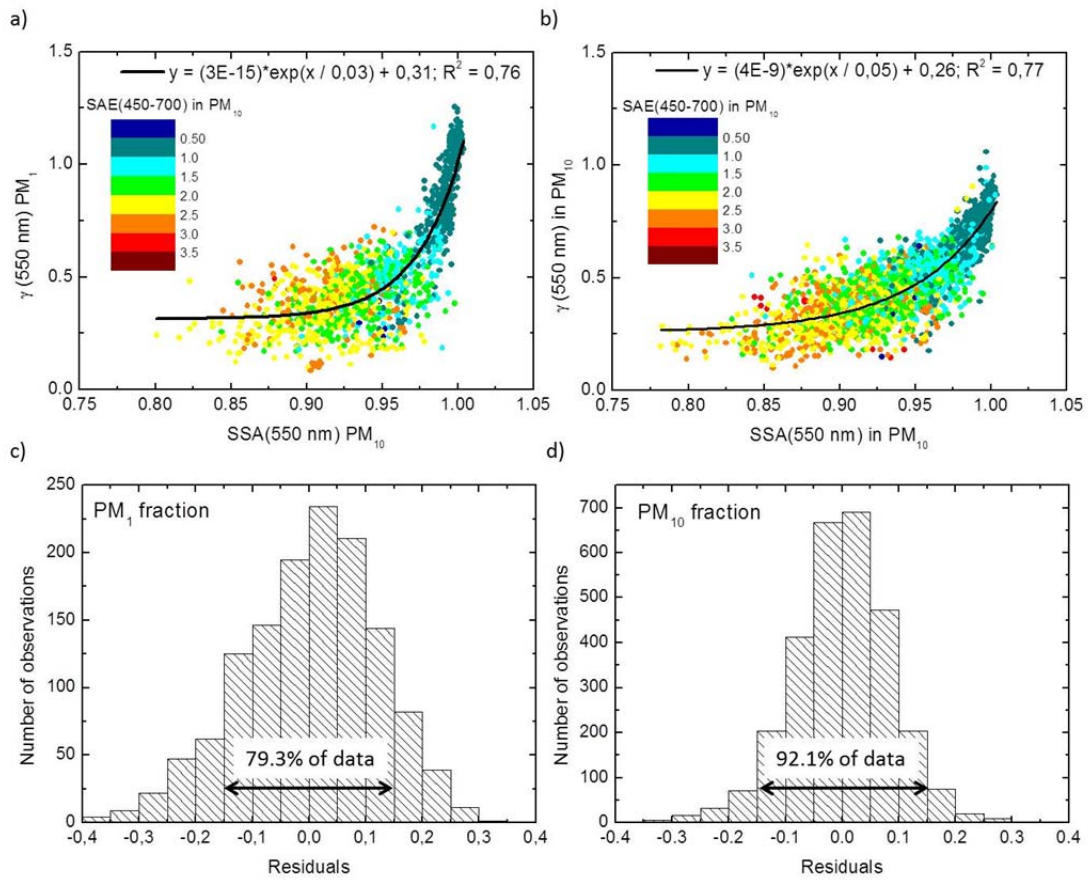
18

19

20

21

1



2

3 Figure 8. γ parameter in PM_1 (a) and PM_{10} (b) versus the single scattering albedo in
4 PM_{10} . The color code corresponds to the scattering Ångström exponent in PM_{10} . An
5 exponential fit has been added to the plot (black line). The residuals of these regressions
6 are plotted as frequency distributions for PM_1 (c) and PM_{10} (d) size fractions.

7

8

9

10

11

12

13

14